Microstructural Study of Two-Phase Marbles in Simple Shear

by

Rachel V. Zucker

Submitted to the Department of Earth, Atmospheric, and Planetary Sciences and the Department of Materials Science and Engineering
In Partial Fulfillment of the Requirements for the Degree of

Bachelor of Earth, Atmospheric, and Planetary Sciences
and
Bachelor of Materials Science and Engineering

At the
Massachusetts Institute of Technology
May 2009

Signature of Author:_____
Department of Earth, Atmospheric, and Planetary Sciences
And Department of Materials Science and Engineering

Certified by:_____
J. Brian Evans
Professor of Earth, Atmospheric, and Planetary Sciences
Thesis Supervisor

Certified by:_____
Samuel M. Allen
POSCO Professor of Physical Metallurgy
Thesis Supervisor

Accepted by:_____
Samuel Bowring
Chair, Committee on Undergraduate Program

Accepted by:_____
Lionel C. Kimerling
Professor of Materials Science and Engineering
Chair, Undergraduate Committee

Microstructural Study of Two-Phase Marbles in Simple Shear

by

Rachel V. Zucker

Submitted to the Department of Earth, Atmospheric, and Planetary Sciences and the Department of Materials Science and Engineering on May 10, 2009
In Partial Fulfillment of the Requirements for the Degree of Bachelor of Earth, Atmospheric, and Planetary Sciences and Bachelor of Materials Science and Engineering

ABSTRACT

Microstructural and textural observations have been conducted on synthetic calcite with 20 wt% quartz deformed in simple shear using transmission electron microscopy and selected-area diffraction. The marbles were deformed at 873, 973, and 1073 K at a stress of 305, 222, and 127 MPa, respectively, and a strain rate of 10^{-4} s^{-1}. The microstructure, shape-preferred orientation (SPO), grain aspect ratios, lattice-preferred orientation (LPO), dislocation densities, and grain sizes were compared to the results of other studies on similar carbonates deformed in triaxial loading, torsion, and simple shear. Microstructures are consistent with other marbles at similar temperatures and stresses, with the only major difference in grain size. The SPO and aspect ratios differ from the theoretical calculations, but are consistent with other marbles. This SPO and aspect ratio is consistent with grains behaving as high-viscosity particles with low-viscosity boundaries. Loading conditions appear to affect the strain at which recrystallization starts, with evidence for new grains at a strain of 3 in this study, compared to minimum strains of at least 4 for others. Dislocation densities are 3.5×10^{13} m^{-2}, 8×10^{13} m^{-2}, and 1.3×10^{14} m^{-2} for the samples at 873, 973, and 1073 K, respectively, and when inserted into a paleopiezometer, the predicted stresses are 347, 257, and 156 MPa, respectively, which is in good agreement with the applied conditions. Among the recrystallized grain size paleopiezometers, rotation recrystallization is a much better match to the data than migration recrystallization, which is consistent with the evidence from SPO and aspect ratios for low viscosity boundaries. Overall, some evidence emerges for material strength differing among different loading conditions, likely caused by differences in LPO. Future studies on the effect of loading conditions on strength are recommended, as this study is very small and only serves as a preliminary investigation.

Thesis Supervisor: J. Brian Evans
Title: Professor of Earth, Atmospheric, and Planetary Science

Thesis Supervisor: Samuel M. Allen
Title: POSCO Professor of Physical Metallurgy

ACKNOWLEDGEMENTS

I would like to thank my advisors Brian Evans and Samuel Allen for their tremendous contributions to my learning and the hours they gave of careful instruction and discussion. Many thanks also to Jorg Renner and Gunter Siddiqi for preparing the samples used in this study. I would also like to thank Jane Connor for her assistance in the writing process, and Yong Zhang for his help while learning microscopy.

TABLE OF CONTENTS

1. INTRODUCTION

Quantifying geologic stress is key to interpreting the structure and history of a region. Since past geologic stresses cannot be measured directly, one must turn to indirect methods to identify deformation conditions. It has been thought for decades that the microstructure of rocks could contain markers that uniquely identify the stress conditions under which they deformed (e.g. Bilby, 1958; Twiss, 1977). These markers are often referred to as paleopiezometers, and the three most commonly-accepted ones are dislocation density, subgrain size, and recrystallized grain size (e.g. Twiss 1977; Kholstedt and Weathers, 1980; Drury and Urai, 1990; Post and Tullis, 1999; de Bresser et al., 2001; Hirth et al., 2005; Mercier et al., 2005; Stripp et al., 2006). Another method for identifying geologic stress is the application of a flow law. If the dominant deformation mechanism can be identified and constraints can be placed on the strain rate, temperature, and pressure, then the strength of the material can be determined (de Bresser et al. 2002). Paleopiezometers and flow laws are often applied in shear zones and faults to determine the magnitude of tectonic stresses (e.g. Briegel and Goetze, 1978; Pfiffner, 1982; Behrmann, 1983; Heitzmann, 1987; Covey-Crump and Rutter, 1989; Burkhard, 1990; Van der Pluijm, 1991; Busch and Van de Pluijm, 1995; Kennedy and Logan, 1997; Molli et al., 2000; de Bresser, 1991; Bestmann et al., 2002; de Bresser et al., 2002; Ulrich et al., 2002). However, these relations are usually empirical and do not always apply to the same mineral with a different microstructure (Goetze and Kholstedt, 1977; Post and Tullis, 1999). In addition, while grossly in agreement, the three paleopiezometers and the flow law for a material typically give different stress values (de Bresser et al., 2002). The lack of generality for flow laws and paleopiezometers greatly limits their utility, and

identifying the necessary modifications to these relations to make them generally applicable has generated much interest (de Bresser et al., 2002; Renner and Evans, 2002). Total strain, strain rate, grain size, deformation history, and secondary phases, to name a few, have been suggested as factors to generalize the flow law (de Bresser et al., 2002). An additional possibility is that the nature of the loading conditions during deformation affects the strength. Traditional rock mechanics tests are done in triaxial loading; however, simple shearing or torsion at similar stresses, strain rates, and temperatures have yielded different microstructures and strengths in the same material (eg. Schmid et al., 1977; 1980; 1987; Casey et al. 1998; Pieri et al. 2001; Rybacki et al., 2003; Barhoorn et al. 2004; Renner et al., 2007). Based on these apparent differences, deeper investigation into the effect of loading conditions on material strength is warranted.

1. 1. Calcite Flow Laws

Calcite is a major rock-forming mineral in the crust. Calcite-rich zones play a particularly important role in tectonic processes because they are often associated with shear zones and thrust faults (Schmid et al., 1977, Bestmann et al., 2000; Burkhard, 1993; Busch and van der Pluijm, 1995). This association indicates that the mechanical behavior of carbonates could be a major contributor to crustal mechanics as a whole. Though carbonate rocks are predominantly composed of calcite, they can also include silicic minerals. Silicate clasts are often observed within calcite mylonites (de Brasser et al. 2002; Herwegh and Kunze 2002). The influence of these non-carbonate phases is a central issue as well in understanding the overall mechanical response of the shear zone.

Because calcite is such an important mineral in tectonic processes, its mechanical properties have been intensively studied (de Bresser et al., 2002). It has been found that no single flow law can fit all the data for calcite over a wide range of temperatures and differential stresses (Rutter, 1974; Schmid et al.; 1977; 1980; 1987; Walker et al., 1990; Renner and Evans, 2002). Instead, the range of conditions studied has been broken up into three regimes (Rutter 1974; Schmid et al. 1977, 1980; Walker et al. 1990; Renner and Evans, 2002): a low-temperature power-law breakdown regime dominated by twinning; a moderate-temperature dislocation climb, cross-slip, and boundary migration regime (de Bresser and Spiers, 1993; Walker et al. 1990); and a high-temperature, low-stress self-diffusion and grain boundary sliding regime (Schmid et al. 1977, 1980; Walker et al. 1990).

The moderate temperature flow regime covers many of the geologically important temperatures, and is most often described by a power law:

$$d\varepsilon/dt = A \, \mathrm{Exp}(-Q/ R T) \, \sigma^n , \qquad (1)$$

where $d\varepsilon/dt$ is the strain rate, A is an empirical value with a possible dependence on thermodynamic conditions, Q is the activation enthalpy for creep, R is the gas constant, T is the temperature, and n is an empirical constant (eg. Schmid et al. 1977; Kholstedt et al., 2005). If this law is valid for a material, then n and Q should be constant over some range of stress and temperature (Renner and Evans, 2002). However, for the moderate temperature flow regime for calcite, experimental data suggests that n and Q actually

vary with grain size (Renner and Evans, 2002; Renner et al., 2002), stress (Renner et al., 2002), temperature (Renner et al., 2002), secondary phase content (Rybacki et al. 2003), or other microstructural or state descriptors (Renner and Evans, 2002; Renner et al., 2002). In addition to a possible dependence on as-of-yet unaccounted for state variables, the empirical constants in the flow law vary greatly among similar carbonate rocks (de Bresser et al., 2002; Renner and Evans, 2002; Renner et al. 2002). The lack of generality in the flow laws for a calcite makes their application in different geologic settings very limited (de Bresser et al., 2002).

The discrepancies between extrapolated experimental flow laws and field observations are also troubling. Experimental flow laws predict grain-boundary diffusion creep as the dominant mechanism for calcite in the upper crust (Walker et al., 1990; Brodie and Rutter, 2000), yet field observations show that dislocation creep is the dominant mechanism (Briegel and Goetze, 1978; Pfiffner, 1982; Behrmann, 1983; Heitzmann, 1987; Covey-Crump and Rutter, 1989; Burkhard, 1990; Van der Pluijm, 1991; Busch and Van de Pluijm, 1995; Kennedy and Logan, 1997; Molli et al., 2000; de Bresser, 1991; Bestmann et al., 2002; de Bresser et al., 2002; Ulrich et al., 2002). de Bresser et al. (2002) highlight the need to include microstructural parameters or state variables in the flow law to hopefully resolve this discrepancy, and to generalize the flow law so that it applies to all calcite-bearing rocks. They point out that a critical area for future work is on the relationship between flow laws and paleopiezometers, and to determine which microstructural variables they are most sensitive to (de Bresser et al., 2002). The present study aims to contribute to the discussion of the dependence of paleopiezometers and

flow laws on loading and microstructure.

1.2. PALEOPIEZOMETERS

The origin of the use of dislocation density as a paleopiezometer lies in dislocation theory, from which it can be shown that the square root of the dislocation density ($\rho_{\perp}$) is proportional to steady-state differential stress (σ) in an isotropic elastic solid, that is,

$$\sigma = c\, \rho_{\perp}^{n} , \qquad (2)$$

where c is an empirical constant that depends on the shear modulus and Burgers vector, and n is typically 0.5 (Bilby et al., 1958). The constants for calcite have been found to be $n = 0.62$ and $c = 10^{-6.21}$ (de Bresser, 1996). This expression holds only for steady-state dislocation densities, and de Bresser contends that there is also a grain-size dependant minimum stress for dislocation creep (de Bresser, 1996).

Based on observations from metallurgical studies (Bird et al., 1969; Luton and Sellars, 1969; Glover and Sellars, 1973, Bromley and Sellars, 1973), Twiss (1977) developed a relationship for dynamically recrystallized grain size (d_{rex}) and subgrain size (d_s) with stress at steady-state creep in minerals. The relationship is a power-law relating steady-state differential stress (σ) and d_{rex} or d_s,

$$\sigma = B\, d^{-n} . \qquad (3)$$

The prefactor, B, depends on the elastic constants of the material and the Burgers vector, and the exponent, n, is empirical. This expression is independent of total strain and temperature. Later studies have posited that d_{rex} and d_s also depend on temperature and/or strain rate (Poirier and Guillopé, 1979; de Bresser et al., 1998, 2001; Drury, 2005). The recrystallized grain size paleopiezometer cannot be universally applicable without modification because of the piezometer's predictions in cases of strain localization. Field observations have shown that in some shear zones, the grain size decreases with proximity to the thrust plane (e.g. White, 1979; Brodie and Rutter, 1988; Austin et al., 2008). The grain size paleopiezometer would therefore predict that stress increases with proximity to the thrust plane. This does not make sense because the pressures probably cannot change significantly on the scale of a few meters, and so other parameters are needed. Other factors that could play a role in the relationship between grain size and stress are recrystallization mechanism (Poirier and Guillopé, 1979; Rutter, 1995), effects of the competition between diffusion and dislocation creep (de Bresser et al., 1998, 2001), subgrain nucleation (Shimizu, 1998), grain-growth rates (Shimizu, 1998), and nucleation-site density (Sakai and Jonas, 1984). There is presently no consensus on the sensitivity of subgrain size or recrystallized grain size to these factors (de Bresser et al., 2002).

Austin and Evans (2007) present an expression for d_{rex} that relates it not to stress, but instead to the rate of work done on the material. The relationship between grain size and stress is given as

$$d_{rex}^{1+p} = C / (p \sigma d\varepsilon/dt), \quad (4)$$

where p and C are constants that can be explicitly solved for using material properties, σ is the differential stress, and $d\varepsilon/dt$ is the strain rate (Austin and Evans, 2007). The relative success of this model suggests that at least in some cases, a paleowattmeter may be more applicable than a paleopiezometer.

The purpose of this study is to provide preliminary insights on the sensitivity of palopiezometers and flow laws to loading conditions. Three samples of synthetic marble with 20 wt% quartz were deformed in simple shear at a confining pressure of 300 MPa at 873, 973 and 1073 K to large strain (~3-4). The resulting microstructures are compared to the microstructures found in previous studies on the same material in torsion (Rybacki et al. 2003) and in triaxial loading (Renner et al., 2007). These results are compared with those from other marbles under the same set of loading conditions, namely the Carrara marble (Schmid et al., 1977; 1980; 1987; Pieri et al., 2001; Barnhoorn et al. 2004) and the Solnhofen limestone (Schmid et al., 1977; 1980; 1987; Casey et al., 1998). The flow laws found in those studies are applied to the simple shear results, and the consistencies and discrepancies are discussed. Paleopiezometers are also applied and discussed, and finally recommendations on promising areas for further study are made.

2. EXPERIMENTAL

2.1. MATERIAL PREPARATION AND DEFORMATION

The synthetic marble used in this study was prepared and deformed by Renner et al. (2007). Reagent-grade $CaCO_3$ powder with 5 μm grain size plus 20 wt% pure quartz were combined and uniaxially cold pressed to 150 MPa. The quartz is angular and averages 3-4 μm in size, though clasts up to 15 μm in size are present (Renner et al., 2007). The cold-pressed bodies were then vacuum-dried at 380 K to remove water. High water fugacity accelerates the reaction between quartz and calcite to form wollastonite, ($CaCO_3 + SiO_2 \rightarrow CaSiO_3 + CO_2$), so removal of water is needed to limit this reaction at high temperature (Renner et al., 2007). The samples were then hot isostatically pressed at 200 MPa and 973 K for 3 hours. Porosity was reduced to 7.5 +/- 0.5 % and the final grain size for calcite was ~13 μm with no change in quartz grain sizes (Rybacki et al., 2003). Calcite grains were roughly euhedral and twin-free, and quartz grains remained angular (Rybacki et al. 2003). All three samples studied contained 80% calcite, 20% quartz, plus trace amounts of 10 – 100 nm wollastonite along grain boundaries (Renner et al., 2007). The hot-pressed material was finally cut into 1.2 mm-thick, ellipsoidal wafers and loaded into a gas-medium apparatus (Paterson Instruments), with an assembly as shown in Figure 1. The alumina driving blocks were precut at a 30° angle to the cylinder axis. The wafers were deformed at a confining pressure of 300 MPa and a shear strain rate of 1.0 x 10^{-4} s^{-1}, up to shear strains of 3-4. The total strain and differential stress for each sample are presented in table 1.

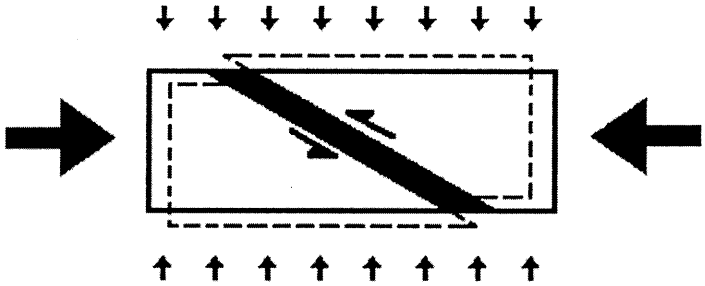

Figure 1. A schematic cross-section of simple shear deformation is shown. The white trapezoids are alumina cylinders cut at a 30° angle. The black band is the ellipsoidal sample. The large arrows show the principal stress, the small arrows show the confining pressure, and the split arrows show the resultant slip direction.

Sample	Temperature (K)	Total Shear Strain	Differential Stress (MPa)
631	873	3.79	305
635	973	3.27	222
632	1073	2.99	127

Table 1. The results of simple shear deformation of calcite with 20 wt% quartz at a strain rate of 10^{-4} s^{-1} are shown.

2. 2. Transmission Electron Microscopy & Data Processing

Transmission electron microscopy (TEM) samples were prepared by focused ion beam (FIB) milling. Each sample is a vertical slice through the wafer, parallel to the shear

direction, measuring approximately 10 μm by 10 μm by 0.25 μm. The foil is separated from the bulk wafer by breaking it off on one edge, thus one side of the foil is less regular in thickness from fracturing. The foil is then carbon-coated and placed on a holey carbon film to support it, which itself is supported by a standard 3 mm-diameter copper grid.

The samples were observed using a Jeol 200CX TEM. Optical studies of the sample are not possible due to the small area of the foils, so low-magnification bright field and dark field images were taken to measure grain and subgrain sizes. The foils are very small, at most 10 μm on a side, so the measured grain sizes represent lower bounds, rather than averages. Higher magnification was used to observe dislocation densities and microstructures. Finally, a survey of grain and subgrain orientations was made using selected-area diffraction (SAD) to distinguish quartz from calcite, find tilt angles, lattice preferred orientation, and to distinguish grain from subgrain boundaries.

The average grain size and subgrain size for each sample were measured using a combination of TEM micrographs and surveying grain orientations using SAD. The sample was imaged at many tilts, lengths were corrected for variations in viewing angle, and the images were superposed so that all boundaries could be seen simultaneously. SAD information was combined with the micrographs to identify the nature of boundaries. Misorientations less than 10° were considered to be subgrain boundaries, and those greater than 10° were grain boundaries. The grain and subgrain sizes were then determined using the line intercept method (Underwood, 1970) along the long and short axes of the grains, then the grain size is given as the diameter of a circle with the same

area as the ellipse defined by the long and short axes. Aspect ratios in this study are given in the same way as Schmid et al. (1987): they are simply the ratio of the short axis length of a grain to the long axis length of a grain. To be consistent with previous work, the strain ellipse is assumed to be equivalent to the ellipse defined by the grain shape.

Lattice preferred orientation (LPO) was measured by a SAD survey of the samples. The crystallographic orientations of half to three-quarters (about 20-40 per foil) of the subgrains present on a foil were determined relative to the shear direction, then the orientations of the crystallographic c-axis were plotted on a stereonet (Wulff plot) for that foil. Many of the subgrains imaged were part of the same grain, so only one point is shown on the stereonet for the grain, rather than a point for each subgrain.

Dislocation densities were measured by the method described by de Bresser (1996). Two overlapping grids rotated at 45° with respect to each other were laid over grains in contrast and the number of intersections of dislocation lines with the grid was counted. Multiple tilts were considered when taking images for measuring dislocation densities, to ensure that all dislocations were visible. Then the total length of the gridlines was found over that area (λ), and the dislocation density ($\rho_\perp$) is given by

$$\rho_\perp = 2N / \lambda t \ , \qquad (5)$$

where N is the number of intersections and t is the thickness of the foil (de Bresser, 1996). When averaging the dislocation densities for a given foil, values were weighted by

area (de Bresser, 1996). *t* was found by imaging the edge of the foil at two different tilts, then using the tilt angles to determine the distance between the two edges.

The samples studied have extremely small areas, on the order of 10 μm x 9 μm, and so there is large uncertainly in these values, and the results of the study should be considered preliminary evidence, rather than substantiated results.

3. RESULTS

3.1. MICROSTRUCTURAL CHARACTERIZATION

3.1.1. Sample 631 – 873 K

Sample 631 shows evidence of a microstructure consistent with high strain and no recrystallization. This foil contains no quartz grains, and consists entirely of calcite ribbons (Figure 2). Grains and subgrains are highly elongated, with aspect ratios (a/c) of 0.19 and 0.52, respectively (Figures 3 and 14). The grains are also heavily deformed, shown by an abundance of dense tangles of dislocations (Figure 4). Grains average 2.6 μm in diameter, and subgrains average 0.85 μm (Figure 13). The dislocation density was determined to be within a factor of two of 1.3×10^{14} m^{-2}, measured over 5.1 μm^2, with a foil thickness of 252 nm. Via diffraction, several grain boundaries were identified as twin boundaries (e.g., Figure 5).

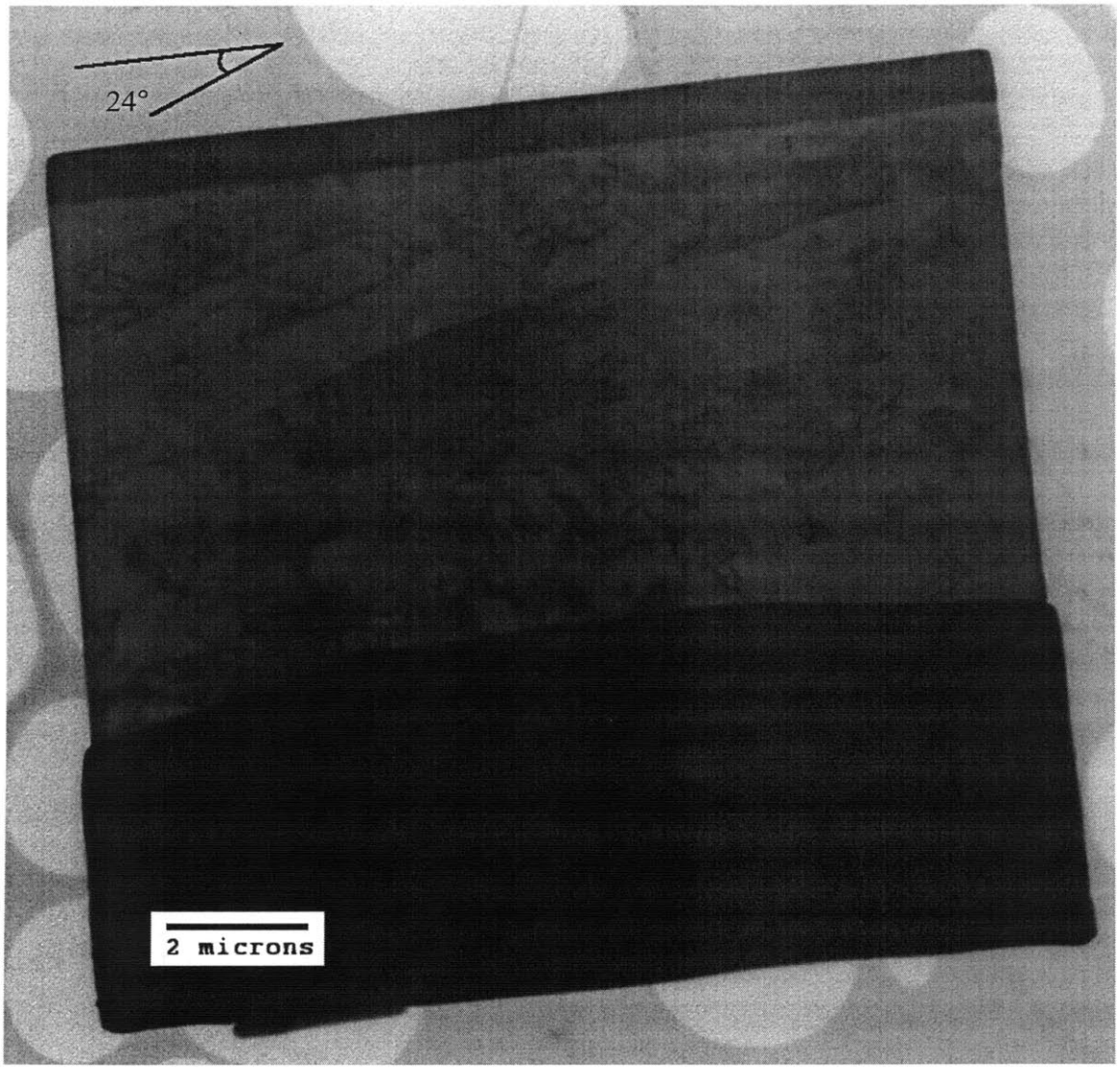

Figure 2. Sample 631 was defomed at 873 K to a total shear strain of 3.79 under a differential stress of 305 MPa. The wedge at the top left shows the theoretical angle between the direction of shearing (parallel to the top sample edge) and the major axis of the finite strain ellipse. The lower third of the sample appears black because it is thicker than the upper portion of the sample, and so it is not electron transparent.

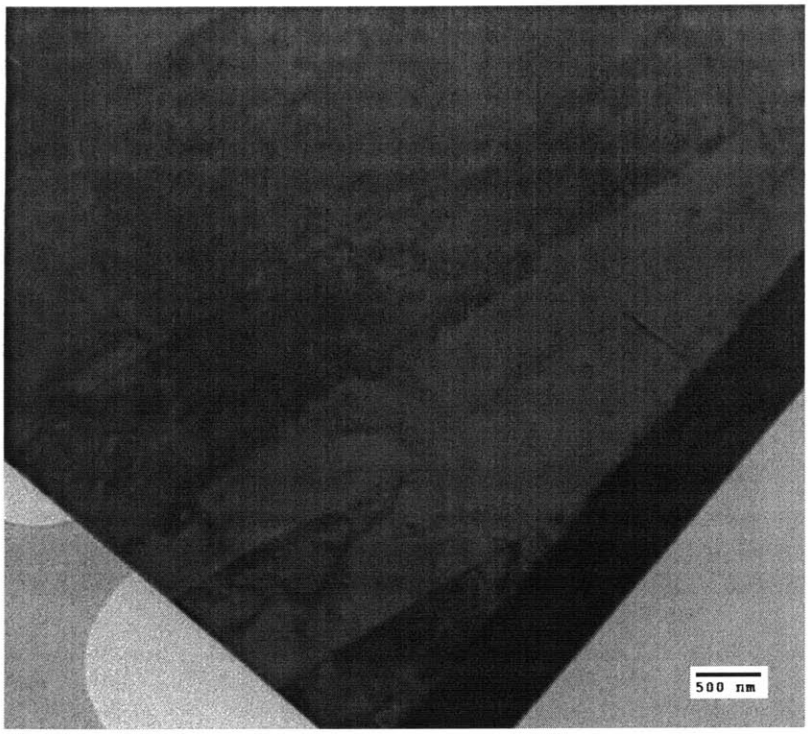

Figure 3. The grains and subgrains in sample 631 are highly elongated and contain dense dislocation networks.

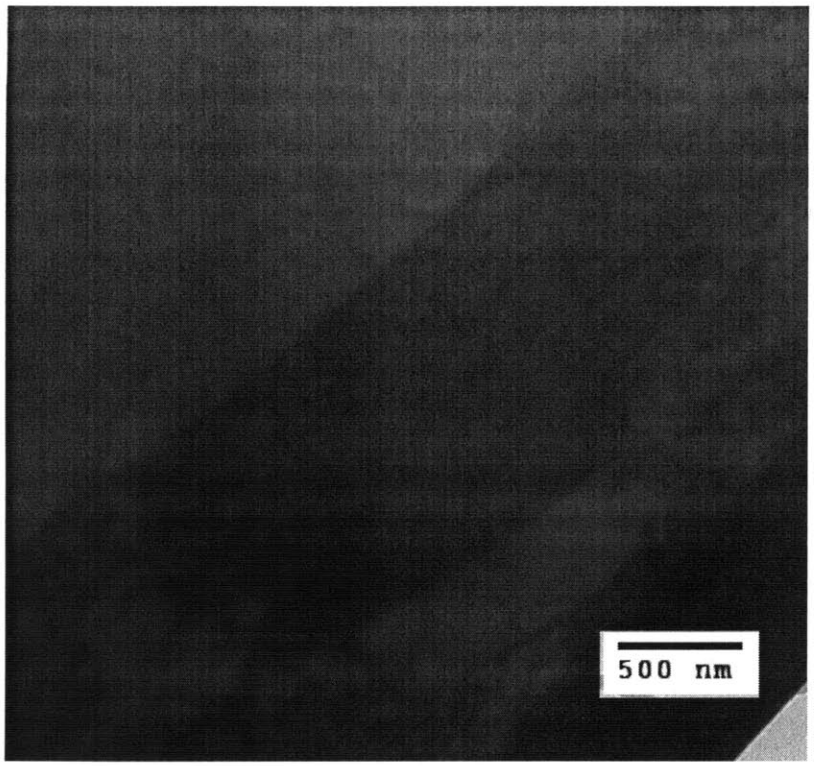

Figure 4. Sample 631 contains dense dislocation tangles. The boundaries on either side of the dark grain are twin boundaries.

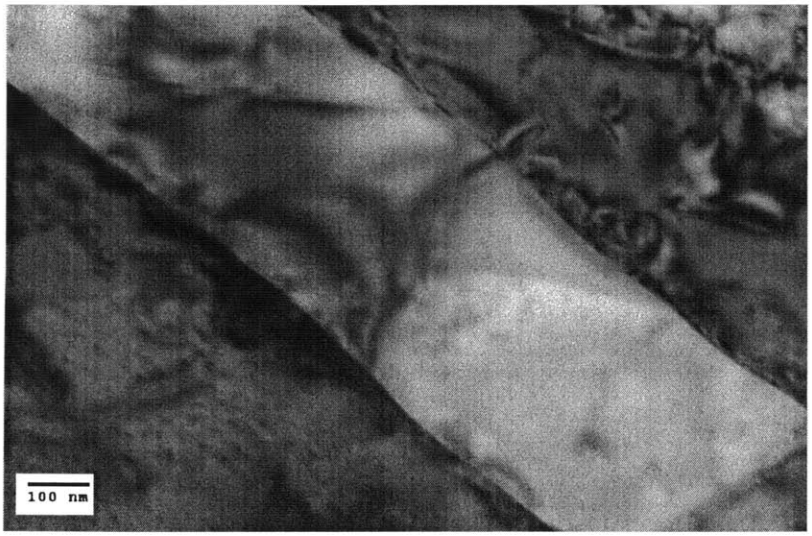

Figure 5. A detailed look at a twin in sample 631.

3.1.2. Sample 635 – 973 K

Sample 635 shows evidence of dislocation creep, resulting in a complicated subgrain structure (Figure 6). There are also dislocation structures on scales smaller than the subgrains (Figure 7). Two quartz grains are present on the foil, one is no less than 10 μm in diameter, and the other is 1.5 μm by 0.5 μm. The quartz grains contain no defects or substructure (Figure 6). The calcite grains present on the foil have an aspect ratio (a/c) of 0.54 and the subgrains have an aspect ratio of 0.79 (Figure 14). The average grain size is 2.0 μm and the subgrain size is 0.82 μm (Figure 13). The dislocation density was observed to be within a factor of two of 8×10^{13} m^{-2} measured over 7.8 μm^2, and the foil thickness was observed to be 260 nm. Many grains contain linear, parallel dislocations, with a regular spacing of approximately 30 nm (Figure 8). It is likely that multiple slip systems coexist in this sample because curved dislocations convex to the shearing direction can also be seen in the same area as the linear dislocations (Figure 9).

Figure 6. Sample 635 was defomed at 973 K to a total shear strain of 3.27 under a differential stress of 96 MPa. The wedge at the top right shows the angle between the direction of shearing (parallel to the top sample edge) and the major axis of the finite strain ellipse. The clear region at the left of the sample is a large quartz grain, as is the small clear grain near the center of the sample (both labelled "qtz"). The darkening present in the lower third of the sample is caused by the sample being thicker in that area from fracturing during sample preparation. The background is a holey carbon film.

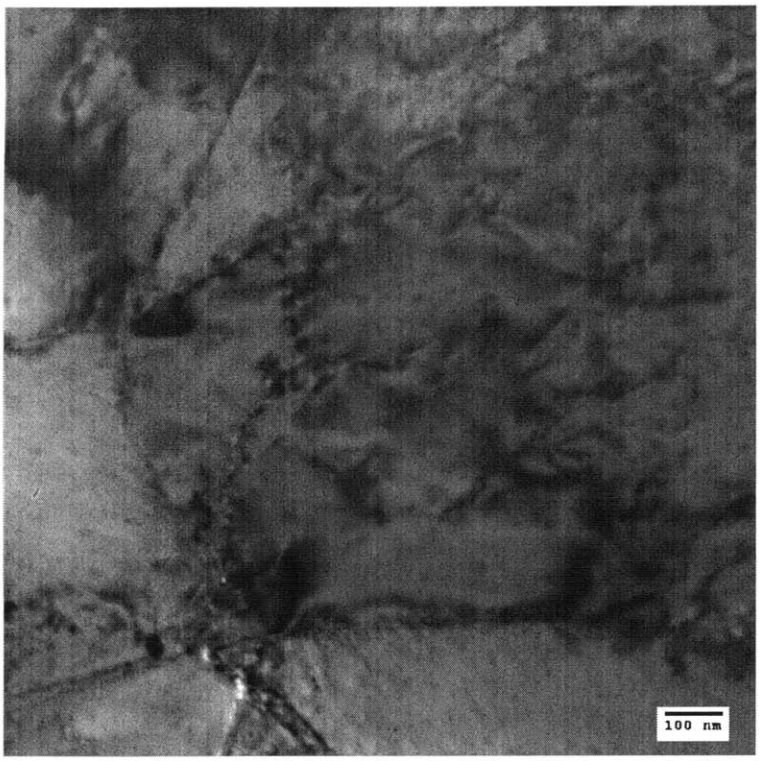

Figure 7. The dislocation structure on scales smaller than that of subgrains in sample 635 is shown.

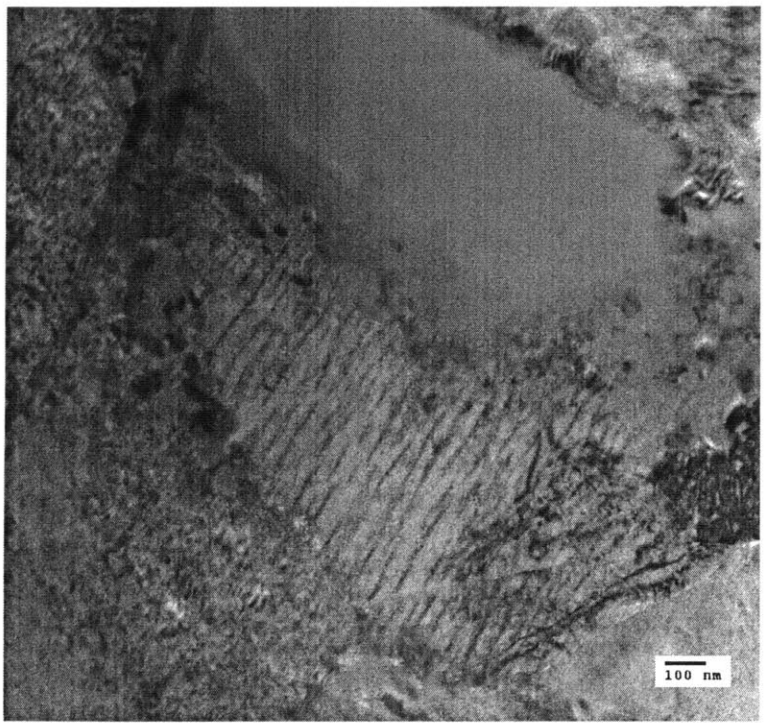

Figure 8. The clear grain at the top is quartz, and the surrounding material is calcite in sample 635. The central subgrain shows dislocation lamellae. The dark, linear feature running NNE in the top left corner is part of the underlying holey carbon film.

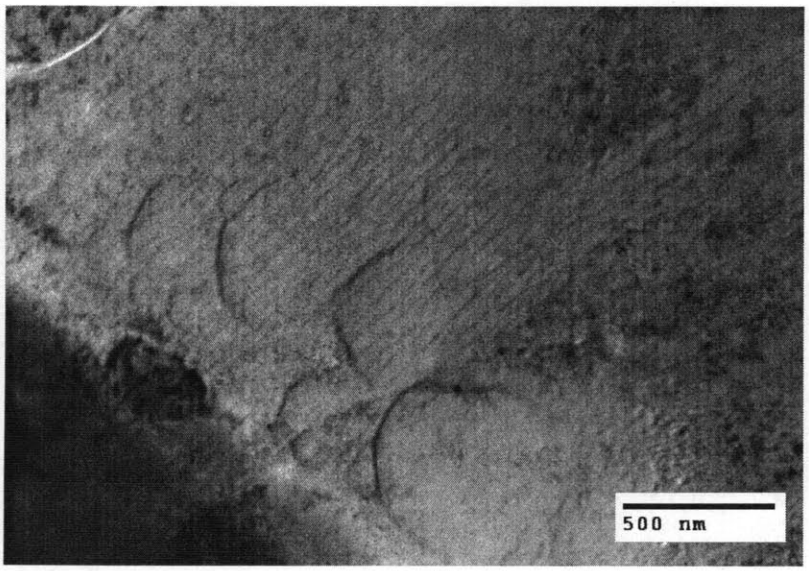

Figure 9. Two sets of dislocations are seen simultaneously in sample 635. It is likely that these dislocations are in two different slip systems, with the dislocation lines in one set trending NE-SW, and the second composed of large dislocation loops convex to the NW direction. The shear direction trends NW-SE and is dextral.

3.1.3. Sample 632 – 1073 K

Sample 632 appears to be partially recrystallized, with nearly equant grains and greatly simplified subgrain structures (Figure 10). No quartz is present in the foil. The grain size is at least 5.3 μm, though it is likely larger because no complete grains are contained on the foil, and the subgrain size is 0.95 μm (Figure 13). The aspect ratios of grains and subgrains are 0.64 and 0.83, respectively (Figure 14). Also, subgrain boundaries lack curvature and are well defined, and triple junctions are easily identifiable with near-120° angles. Other grains contain irregularly-shaped subgrains and complicated dislocation structures, indicting that they are not recrystallized grains (Figure 10). These grains also have concave boundaries. The dislocation density was observed to be within a factor of two of 3×10^{13} m^{-2} in the recrystallized grains measured over 7.2 μm^2 and 4×10^{13} m^{-2} in old grains measured over 5.1 μm^2. These dislocation densities are the same within the margin of error, and so it is assumed that these represent equilibrium dislocation densities and the dislocation density for the foil is taken to be 3.5×10^{13} m^{-2}. The foil thickness is 242 nm. In this sample, 10-20 nm-sized, unidentified prismatic inclusions were found within the heavily deformed grain (Figure 11). These inclusions are likely contamination from preparing the material because wollastonite has a massive habit and appears dark on TEM micrographs, thus ruling out wollastonite (Rybacki et al. 2003). Also, the inclusions are within a calcite grain, with no nearby quartz.

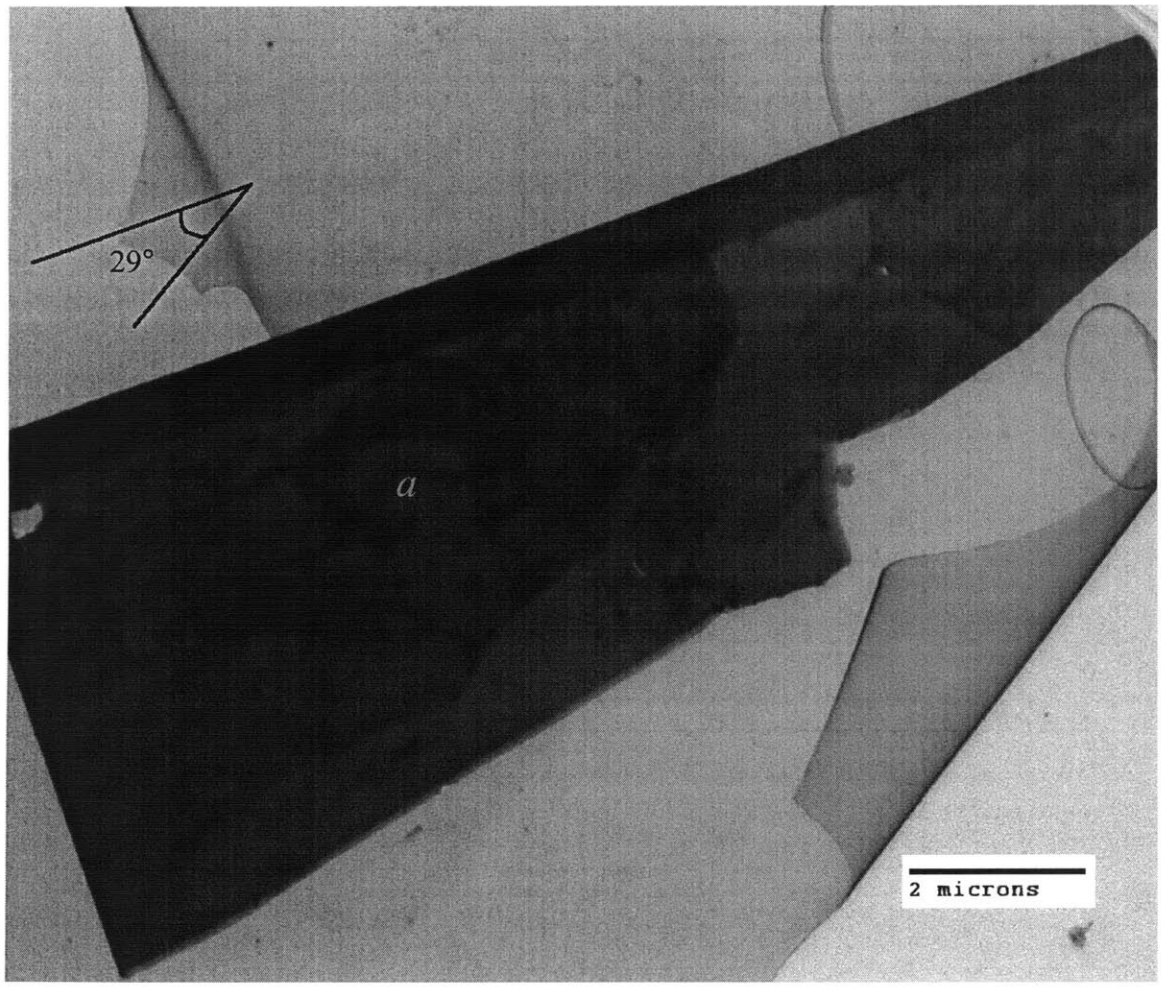

Figure 10. Sample 632 was defomed at 1073 K to a total shear strain of 2.99 under a differential stress of 55 MPa. The wedge at the top left shows the theoretical angle between the direction of shearing (parallel to the top sample edge) and the major axis of the finite strain ellipse. Most of the grains are recrystallized; however, the large grain at the center-left of the sample (labelled *a*) has not been recrystallized. It contains a complicated dislocation structure. Note the concave boundaries around this grain, consistent with growth of recrystallized grains.

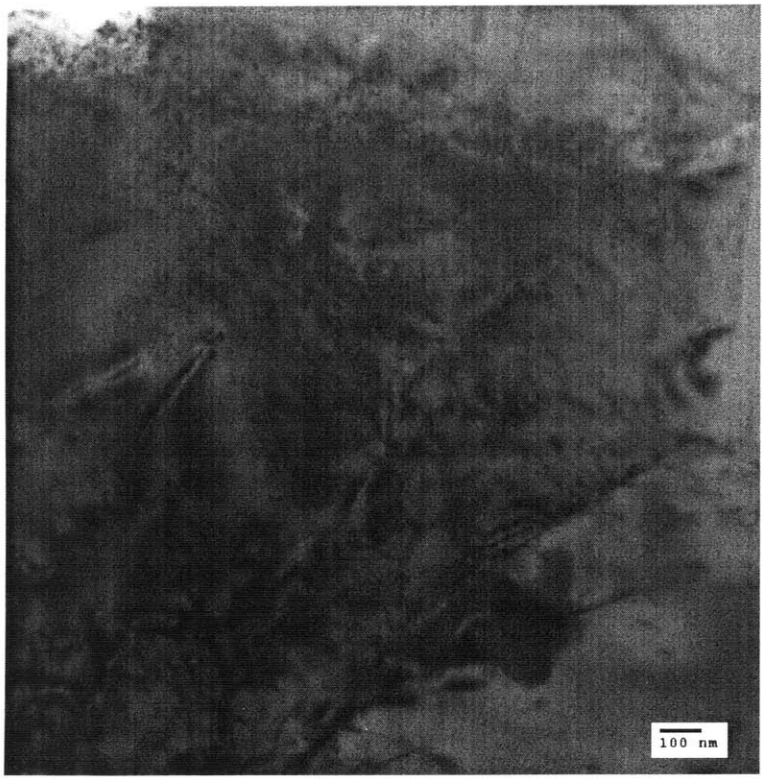

Figure 11. Dislocations in a recrystallized grain from sample 632 are shown. Some of the small black dots are damage from the electron beam.

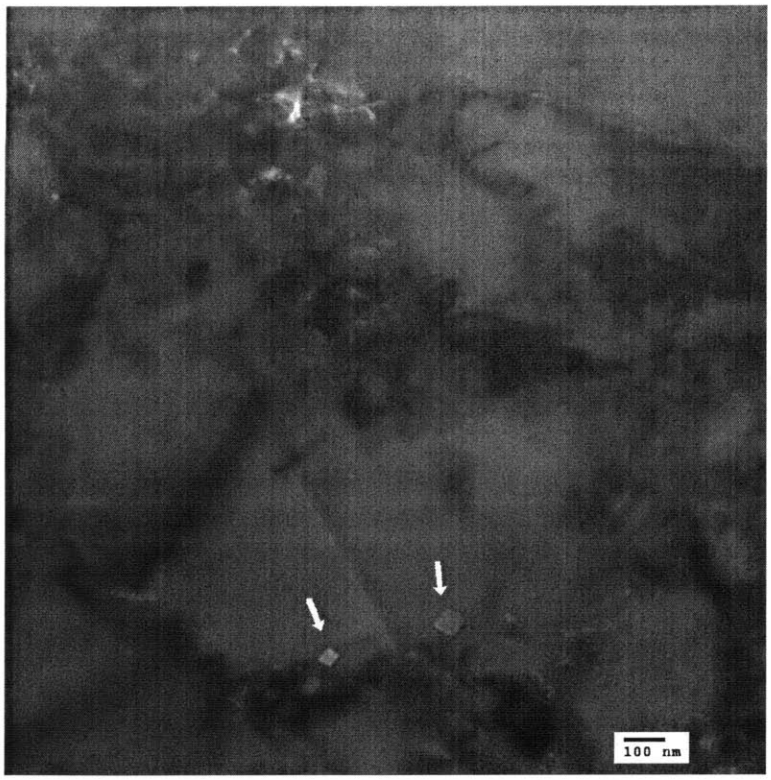

Figure 12. Unientified inclusions are present in sample 632. They are probably not wollastonite because no quartz grains are present and wollastonite does not have a prismatic habit, but instead appears dark and massive on TEM micrographs.

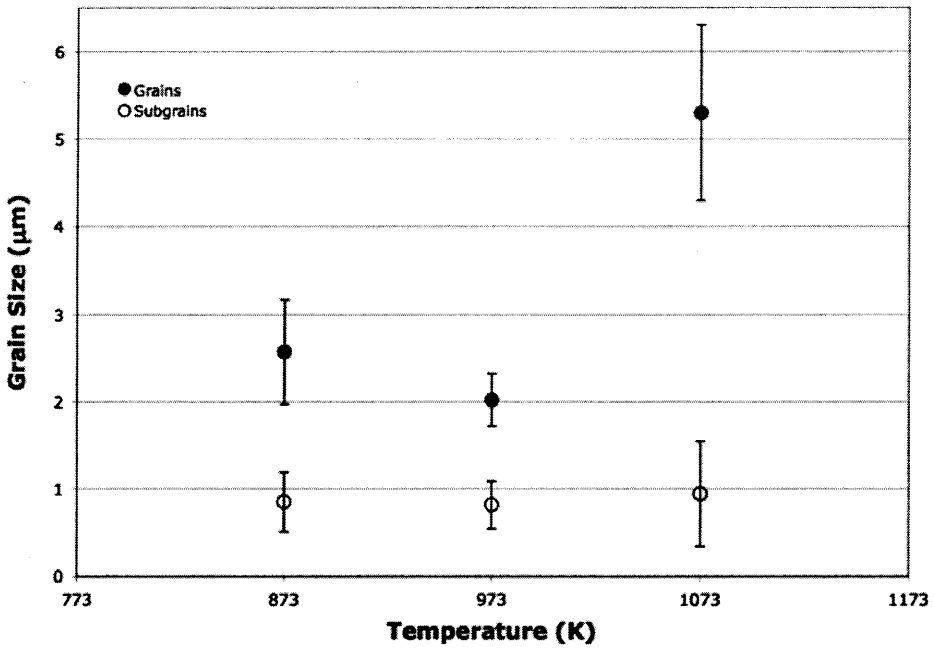

Figure 13. The average size of grains and subgrains in each sample is shown. Subgrain sizes are open symbols, grain sizes are filled symbols.

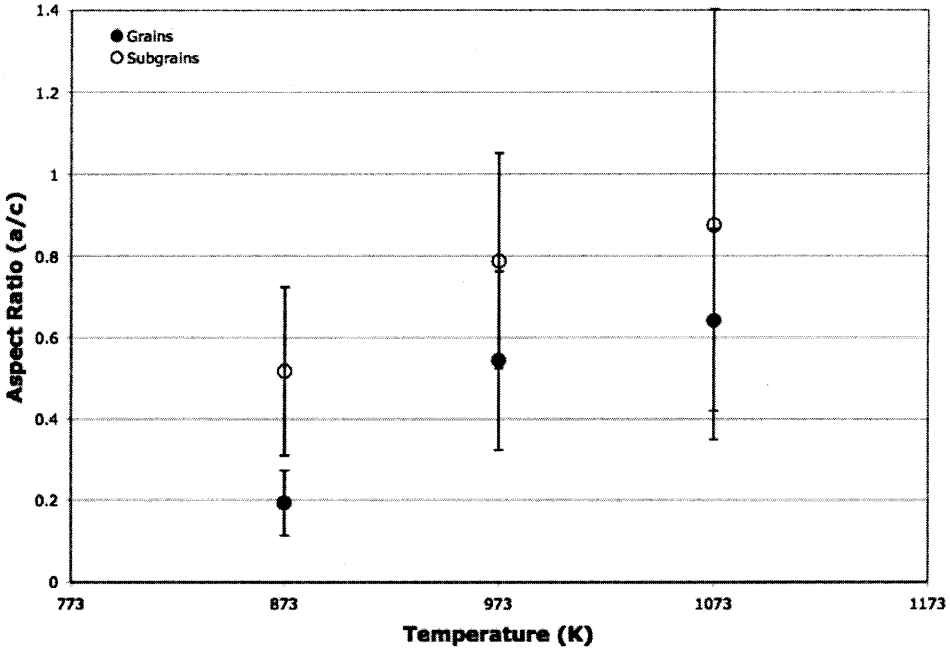

Figure 14. The aspect ratios of grains and subgrains in each sample are shown. Open symbols are subgrains, filled symbols are grains.

3.2. TEXTURE AND PREFERRED ORIENTATIONS

To estimate whether grains have a crystallographic preferred orientation, the direction of the c-axis (0 0 0 1) was plotted on a stereonet (Wulff plot) for each sample (Figure 15a). The number of grains on the foils is very small, so each sample provides only a handful of orientations. None of the samples provide sufficient data to contour the pole figures. The only discernable trend is that the c-axis is preferentially in the plane containing the principal stress and the shear direction (Figure 15a). The lowest temperature sample, 631, shows some hints of a preferred c-axis direction perpendicular to the greatest

compressive stress, σ_1 (Figure 15a1); however; the data set is too small to say definitively.

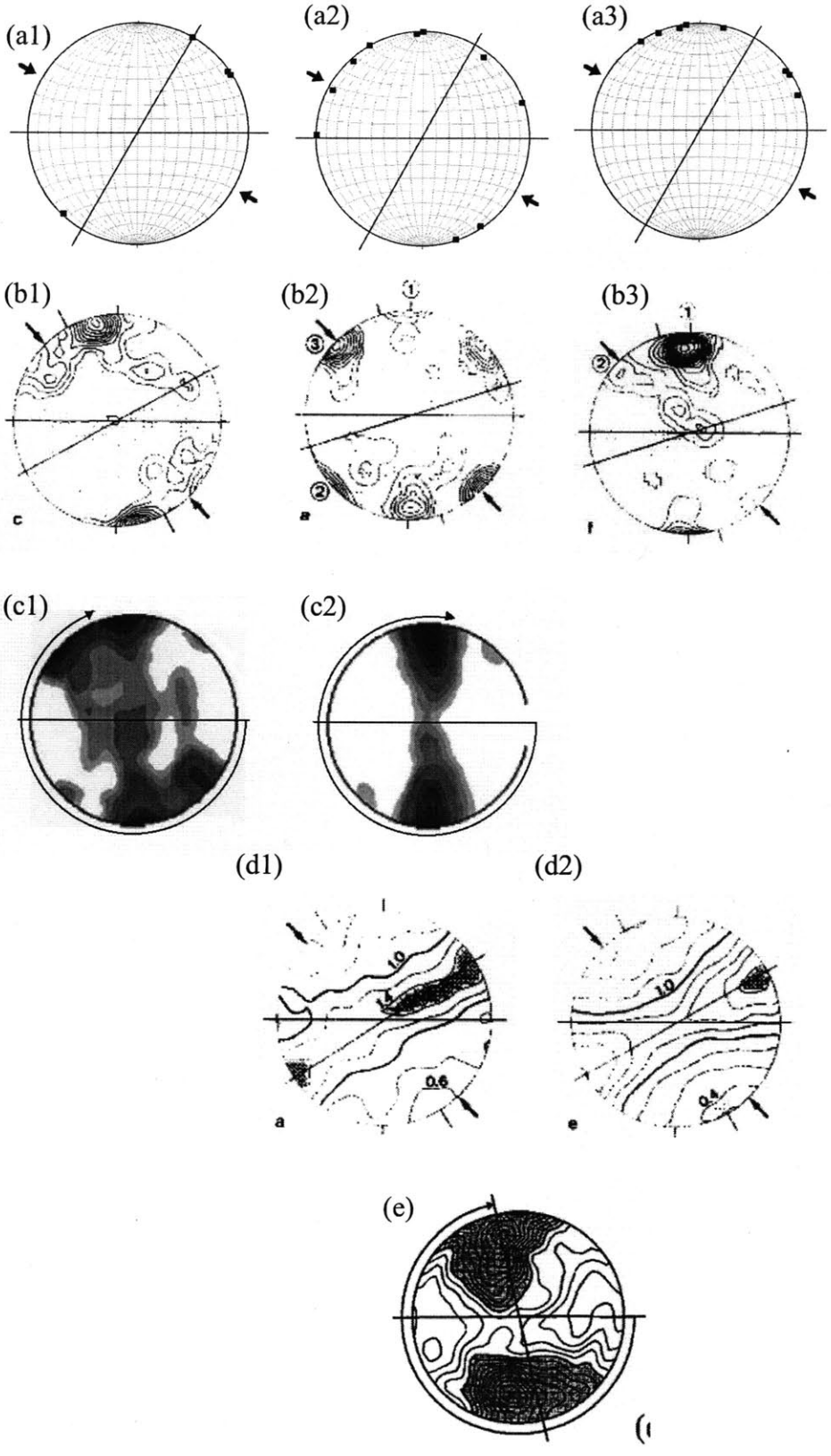
(a1)
(a2)
(a3)
(b1)
(b2)
(b3)
(c1)
(c2)
(d1)
(d2)
(e)

Figure 15. Pole figures for the c-axes (0 0 0 1) of three marbles in two different loading conditions are compared. In all cases, projections are equal area and the shear plane is represented by the horizontal line. In simple shear (parts (a), (b), and (d)), the inclined line shows the plane of greatest finite shortening and the arrows show the direction of the greatest compressive stress, σ_1. In torsion (parts (c) and (e)), the shear plane is the horizontal great circle, and the arrow indicates the direction and amount of twisting. (a) Stereographic projections (Wulff plots) are shown for synthetic marble in simple shear (this study) at 873 (a1), 973 (a2) and 1073 K (a3). Stereographic projections are equivalent to pole figures, except pole figures show contours of the density of axes, while stereographic projections are not contoured. The data are presented this way because there is so little data that contouring would be uninformative. (b) The Carrara marble in simple shear (Schmid et al., 1987) at 873 (b1), 973 (b2) and 1073 K (b3). (c) The Carrara marble in torsion (Barnhoorn et al. 2004) for strains of roughly 4 at 873 (c1) and 1000 K (c2). (d) the Solnhofen limestone in simple shear (Schmid et al. 1987) at 973 (d1) and 1073 K (d2). (e) The Solnhofen limestone in torsion (Casey et al., 1998) for strain of roughly 3 at 750 K.

4. DISCUSSION

4.1. LATTICE-PREFERRED ORIENTATION (LPO)

To first order, the preliminary LPO results for the synthetic marble deformed in simple shear agree with the results of previous work on other marbles in simple shear (Figure 15). The Carrara marble shows a strong LPO in simple shear with the c-axes limited to the periphery of the pole figure, regardless of flow regime (Schmid et al., 1987). Evidence of this same pattern is observed in the synthetic marble (Figures 15a and 15b). The Solnhofen limestone shows a LPO fairly different from that of the Carrara marble in simple shear (Schmid et al., 1987). Instead of decorating the periphery, the c-axes cluster along the plane normal to σ_1, with a preference for the margin of the pole figure (Schmid et al. 1987). The synthetic marble may show this LPO at 873 K; however, more data is needed to substantiate or refute this possibility. In torsion, the Carrara marble and Solnhofen limestone show similar c-axis LPOs, which are generally weaker and spread more evenly across the pole figure, with a preference for the plane normal to the shear direction (Casey et al., 1998; Barnhoorn e al. 2004). The synthetic marble shows little similarity with the torsion LPOs, and so speculatively, it appears that the LPO of the synthetic marble in simple shear is consistent with results from other studies in simple shear, and is different from those obtained in torsion.

4.2. FLOW LAWS

By considering the microstructure of the samples, the applicability of the various flow laws for calcite can be gauged. The flow laws considered are those by Rutter (1974) and

Schmid et al. (1977; 1980; 1987) for the Carrara marble and Solnhofen limestone, Heard and Rayleigh (1972) for the Yule marble, and Rybacki et al. (2003) for synthetic marble in torsion.

Sample 631 was deformed at 873 K under a differential stress of 305 MPa. The microstructure contains both twin boundaries and dislocation structures. This temperature and stress correspond to the boundary of the twinning flow regime and dislocation creep regime in the Carrara marble, identified by Rutter (1974) and Schmid et al. (1977; 1980). Applicability of the Carrara marble flow law to the synthetic marble therefore seems reasonable, given the similarities in plasticity mechanisms. The deformation conditions for this sample fall within the twinning flow regime identified for the Solnhofen limestone and Yule marble in triaxial loading (Heard and Raleigh, 1972; Schmid et al. 1977). A twinning-dominated plasticity mechanism is inconsistent with the observed microstructure because there is clear evidence of dislocation creep, so reasonable stress predictions from the Solnhofen limestone and Yule marble flow laws are unexpected.

Sample 635 was deformed at 973 K under 222 MPa of differential stress. The observed microstructure showed clear evidence of dislocation creep, no twinning, and no recrystallized grains were present in the foil. Grain boundaries are irregular and interleaved. The experimental conditions fall within the dislocation creep regime identified by Schmid et al. (1977; 1980) for both the Carrara marble and the Solnhofen limestone. The Yule marble flow law put these conditions in the twining regime (Heard

and Raleigh, 1972). The microstructure of sample 635 is consistent with dislocation creep and not with twinning, so the Carrara and Solnhofen flow laws should apply to the synthetic marble, but not the Yule flow law. In the dislocation creep regime, grain boundaries are highly mobile, resulting in the interleaving of different grains and particularly small subgrains along grain boundaries (Schmid, 1980, Rybacki et al., 2003). This pattern was also observed in the sample, further substantiating the match in microstructures.

Sample 632 was deformed at 1073 K under 127 MPa of differential stress. The microstructure shows a combination of old grains with complicated dislocation structures and recrystallized grains with far simpler structures. The deformation conditions fall within the dislocation creep regime for the Solnhofen limestone, Yule marble, and Carrara marble, following Schmid et al. (1977; 1980) and Heard and Raleigh (1972). The microstructures are also consistent, with the natural marbles and the synthetic both showing recrystallized grains and dislocation structures.

Rybacki et al. (2003) developed a flow law for the same synthetic, two-phase marble in torsion. Rybacki et al. (2003) report that dislocation creep dominates in the range of temperatures examined in this study. Because their studies was performed on the same material, it is expected that their flow law will be the best match for synthetic marble in simple shear for all three samples.

Given these expectations, the success of each flow law can be examined. The flow laws were converted from triaxial geometry to shear geometry (when appropriate) using the expression developed by Schmid et al. (1987). The conversion assumes Von Mises behavior (Schmid et al., 1987). The strength predicted for each sample using these flow laws is shown in table 2. As expected, the Yule marble flow law is a poor match for the synthetic marble because of the mismatch in microstructure. Also as expected, the flow law by Rybacki et al. (2003) is the best match because it was developed for the same material. However, the flow laws for natural marbles all grossly underestimate the stress, which is not expected because they have equivalent deformation mechanisms, temperatures, and stress regimes. This result is consistent with the conclusion made previously by others (Renner and Evans, 2002; Renner et al. 2002; de Bresser et al. 2002) that the assumption that calcite obeys a diffusion-creep power-law is not valid. Given the results in Table 2, grain size appears to systematically increase with decreasing stress estimates. This Hall-Petch like, grain-size strengthening behavior has been noted before (Renner and Evans, 2002; Renner et al. 2002; de Bresser et al. 2002). Another outstanding possibility is that the quartz content of the synthetic marble has caused significant strengthening, and further studies are needed to quantify the effect of the addition of higher viscosity phases.

Sam-ple	Temp-erature (K)	Experiment Differential Stress (MPa) Grain size = 3 μm	Calculated by flow law for Synthetic Marble with 30% quartz in Tosion* Grain size = 5 μm	Calculated flow law for Solnhofen Limestone (MPa)** Grain size = 4 μm	Calculated by flow laws for Carrara Marble (MPa)** Grain size = 200 μm	Calculated by flow law for Yule Marble (MPa)*** Grain size = 300 – 400 μm
631	873	305	374	169	89	61
635	973	222	143	143	64	35
632	1073	127	105	104	44	19

* Flow law parameters are taken from Rybacki et al. 2003.
** Flow law parameters are taken from Schmid et al. 1980.
*** Flow law parameters are taken from Heard and Raleigh 1972.

Table 2. A comparison of the empirical flow laws developed for calcite with experimental data for simple shear experiments, using a conversion by Schmid et al. (1987) of the flow law from triaxial to simple shear geometry, assuming a von Mises failure envelope.

Beyond the potential for grain size dependence, there is also evidence of loading dependence. The torsion flow law overestimates the stress for the colder samples and underestimated for the hotter sample. This type of offset could be due to a number of things. First, there are assumptions about the yield envelope built in to the flow law from Rybacki et al. (2003). Data processing requires assumptions that the yield envelope is Von Mises, and that it is at steady state. Discrepancies between the torsion data and this study could be due to these assumptions not holding. Another possibility is that the different loading conditions require different flow law parameters. The slight difference in grain size is an unlikely candidate for the discrepancy because the stress for the colder sample should have been underestimated in that case, not overestimated. In addition, the

strength increase provided by increasing quartz content saturates at 20 wt%, so the flow law parameters are nearly identical for 20 wt% and 30 wt% (Rybacki et al. 2003). Thus, the poor correlation between torsion and simple shear loading could be due to differences in LPO. The comparisons between the LPO in simple shear and torsion for the Carrara marble and Solnhofen marble show distinct LPOs, and therefore differences could also be expected for the synthetic marble as well. However, the relative magnitudes of changes to the flow law from differences in LPO versus error introduced by assumptions in the torsion data processing are unknown. To determine whether the difference in predicted strength is an artifact of the yield surface assumption or a real effect of a difference in LPO requires further investigation.

4.3. Aspect Ratio and Shape-Preferred Orientation (SPO)

To further investigate deformation mechanisms and microstructutral properties, it is useful to consider the aspect ratio and shape-preferred orientation (SPO) of the samples. The aspect ratios measured in the synthetic marble in simple shear are compared to the aspect ratios observed in torsion by Rybacki et al. (2003) in Figure 16. Rybacki et al. (2003) have shown that the grains in the undeformed material are initially euhedral, and extend along the major axis of the strain ellipse until reaching a minimum aspect ratio (a/c) of ~0.2 at strain ~4-5, then recrystallization activates and the aspect ratio increases again (Rybacki et al., 2003). The relationship between aspect ratio and shear strain appears independent of temperature (over the range 873 – 1073 K) and quartz content (for full data set, see Rybacki et al. 2003). Comparing the results of the present study over a similar temperature range to the torsion data, there is evidence of different

behaviors of aspect ratio with loading conditions. The 1073 K sample from this study shows strong evidence of being recrystallized, yet the shear strain was only 2.99. The torsion data suggests that recrystallization should not be this extensive at such a low strain. A possible explanation is that the different loading conditions result in different activities of the various slip systems, and that the aspect ratio of the grains produced is directly affected. Such a relationship has already been suggested by the differences in LPO produced during simple shear and torsion experiments in both Carrara marble and Solnhofen limestone (Schmid et al., 1987; Casey et al., 1998; Barnhoorn et al., 2004). It is important to note that the grain size measurement is very uncertain for this sample due to its small area, and this relationship may not be true when a more representative area is considered. However, it does indicate that further investigation is warranted into a possible change in the onset of recrystallization due to loading conditions.

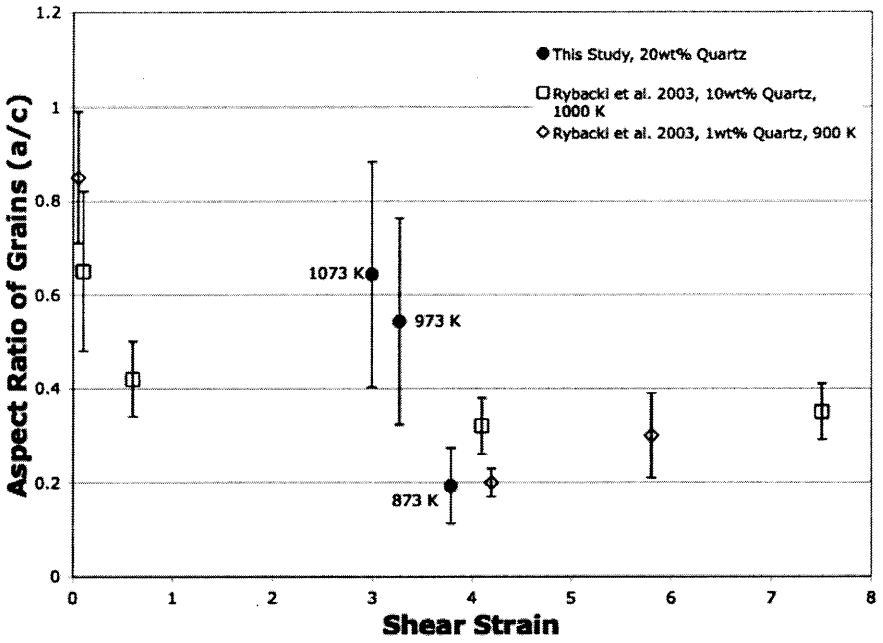

Figure 16. The aspect ratios of grains deformed in simple shear and those deformed in torsion (Rybacki et al., 2003) are compared. Despite being deformed at similar temperatures, the simple shear samples appear to have a different behavior.

The angle between the shear plane and the major axis of the strain ellipse can be used to estimate the amount of shear strain a natural rock has undergone, which is a critical step towards determining strain rate and ultimately shear stress and material strength (de Bresser et al., 2002). The theoretical strain ellipse angle is related to the shear strain by

$$\mathrm{Tan}(2\,\Phi) = 2 / \gamma\,, \qquad (6)$$

where Φ is the theoretical angle between the major axis of the strain ellipse and the shear direction and γ is the shear strain (Rybacki et al., 2003). To test whether there is any difference between torsion and simple shear loading in the strain measured by this method, the theoretical and observed angles were compared for the Carrara marble, the Solnhofen Limestone, and synthetic marbles with varying quartz content (Figure 17) (Barnhoorn et al., 2004; Schmid et al., 1987; Rybacki et al. 2003). The ellipse axis angle appears independent of quartz content and temperature. Torsion experiments for the Carrara marble consistently have larger than predicted angles, while the synthetic torsion experiments consistently match the theoretical angle (Barnhoorn et al., 2004; Rybacki et al., 2003). The Carrara torsion data instead follow material lines through shear, and not the major axis of the strain ellipse (Barnhoorn et al., 2004). In simple shear, observed angles are consistently below the theoretical angles, indicating that grains are rotating more than the theoretical strain ellipse (Schmid et al., 1987).

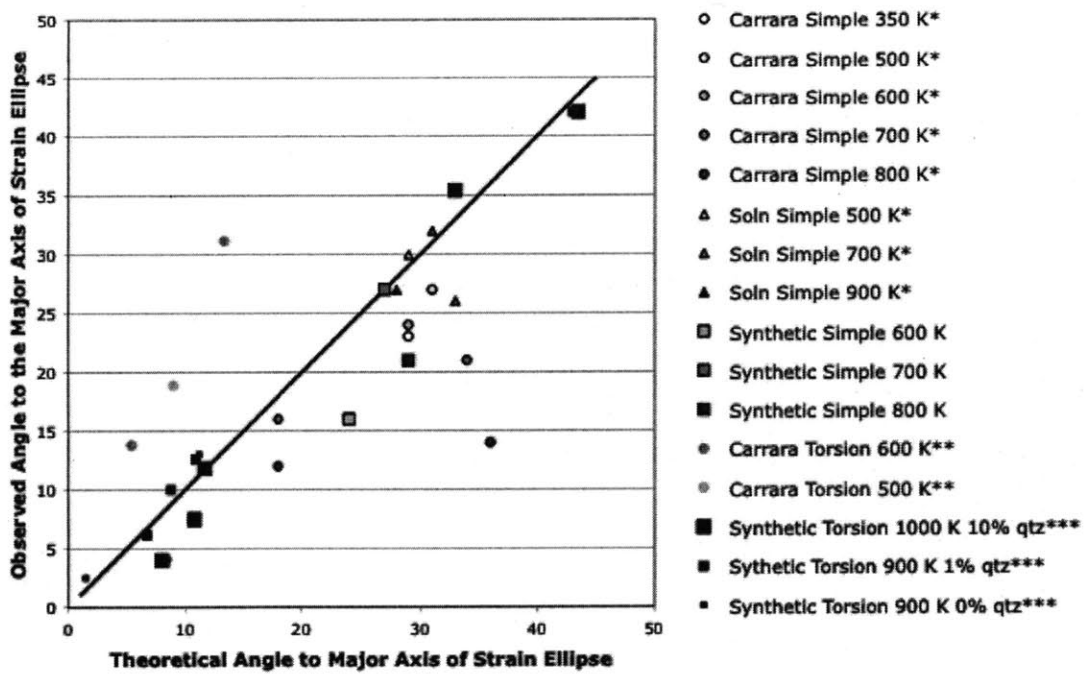

* Carrara marble and Solnhofen limestone simple shear data is from Schmid et al., 1987.
** Carrara marble torsion data is from Barhoorn et al., 2004.
*** Synthetic marble torsion data is from Rybacki et al., 2003.

Figure 17. The theoretical and observed angles between the shear direction and major axis of the strain ellipse are compared for torsion and simple shearing. Filled symbols are for simple shear loading and open symbols are for torsion loading. The size of the marker for the synthetic marble indicates the quartz content. The observed angle in simple shear experiments tends to be small relative to the theoretical angle.

The combination of a larger-than-expected aspect ratio and a smaller-than-expected strain ellipse angle is consistent with grains behaving as higher viscosity particles in a lower viscosity matrix (Ghosh and Ramberg, 1976; Schmid et al., 1987). This is evidence for either grain-boundary sliding as an active deformation mechanism, or the subgrains at the edges of grains accommodating slip and insulting the interior of the grain from straining

as much (Schmid et al., 1987). This has been observed in the Carrara marble as well (Schmid et al., 1980; 1987). Whether this is rigorously true for the synthetic marble remains to be investigated.

4.4. PALEOPIEZOMETERS

Using the parameters defined by de Bresser (1996), the stress of deformation was calculated using the free dislocation density in the samples. The results of this paleopiezometer are shown in Table 3. The dislocation densities do fairly well as a piezometer, getting within 12% of the actual stress for the samples. The consistent overestimation may be coincidence due to the very small areas observed, or it could be, again, due to differences in loading conditions. De Bresser (1996) developed the parameters in the paleopiezometer for triaxial data, and there may be a difference in which slip systems are active. A more thorough investigation into the difference is warranted, not only for this material, but for other carbonates in different loading conditions.

Sample	Average dislocation density (m^{-2})	Experimental Differential Stress (MPa)	Calculated Stress (MPa)
631	1.3×10^{14}	305	347
635	8×10^{13}	222	257
632	3.5×10^{13}	127	156

Table 3. The predicted differential stresses for synthetic marble using the paleopiezometer parameters identified by de Bresser (2006) are compared to the actual stresses.

To test the applicability of the paleowattmeter to calcite in simple shear, the parameters determined by Austin and Evans (2007) are compared with recrystallized grain size paleopiezometers (Figure 18). The paleopiezometers developed by Rutter (1995) are for a rotation recrystallization mechanism and a migration recrystallization mechanism. Only sample 632 contained recrystallized grains, so only this datum can be compared with the paleopiezometer curves. The paleowattmeter applies for all grains, not just recrystallized grains, because it is derived from the energy stored in the grain boundaries, rather than grain sizes (Austin and Evans, 2007). It appears that the present data set is inconclusive, with perhaps a slightly better match to the paleopiezometer, though both the wattmeter and piezometer curves are largely outside the error bars of the data. The poor agreement between both stress measures and the data could be due to the small size of the TEM foil. The foil is at most 10 μm x 8 μm, and that severely limits the number and size of grains that can be measured. These grain size measurements should therefore be considered a lower bound, rather than an average. The only conclusion that can be tentatively drawn is that if the paleopiezometer applies to this material, then it is likely undergoing rotation recrystallization, rather than migration recrystallization.

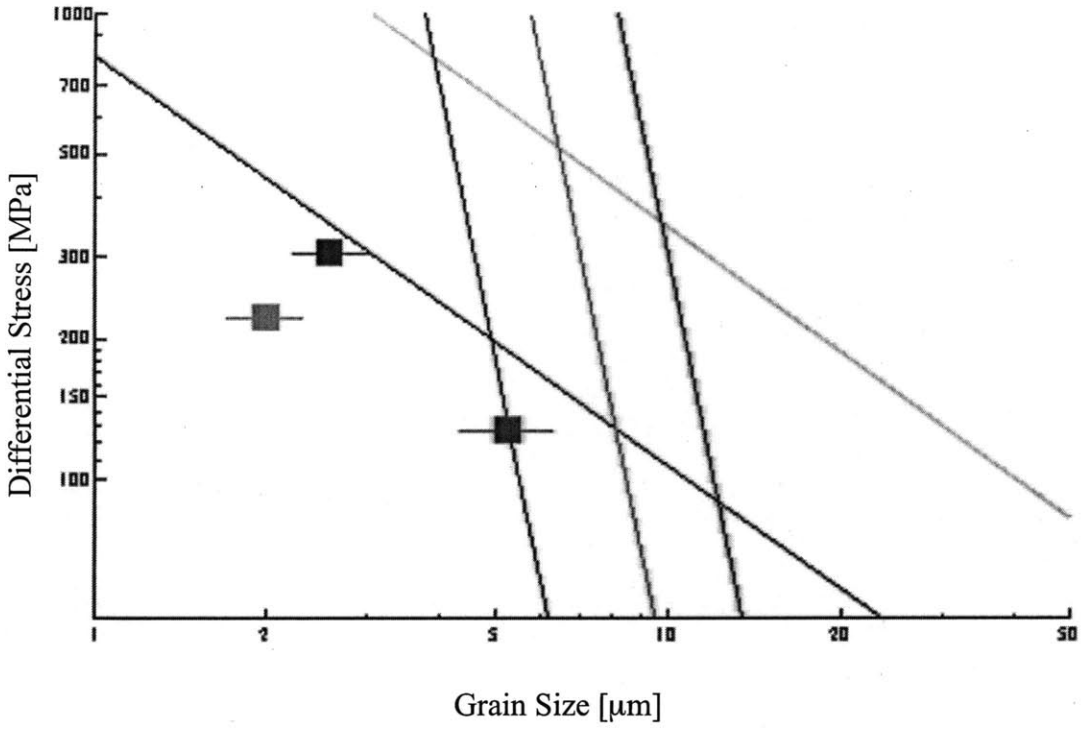

Figure 18. A comparison of paleopiezometers and paleowattmeters. The black line is rotation recrystalization (from Rutter, 1995), the gold line is boundary migration recrystallization (from Rutter, 1995), and the colored lines are the paleowattmeters for calcite after Austin and Evans (2007) for 873 K (blue), 973 K (green) and 1073 K (red).

5. CONCLUSIONS

The relationship between deformation conditions and state variables has proven difficult to quantify in calcite. While power-law dislocation-creep describes the moderate-temperature behavior of calcite to first-order, systematic discrepancies among even similar marbles have been difficult to reconcile. Many candidate parameters to incorporate into flow laws and paleopiezometers have been identified to accurately relate

stress and material properties, yet the full suite of candidate parameters is still unknown. Comparing the microstructural properties, lattice-preferred orientations (LPOs), grain sizes, shape-preferred orientations (SPOs), aspect ratios, and dislocation densities in marbles deformed triaxially, in simple shear, and in torsion has shed some light on the sensitivity of flow strength to the loading conditions. Though the scale of observations in this study is only sufficient to count as a preliminary investigation, trends began to emerge. Qualitative microstructural charcteristics are reasonably consistent among different marbles and loading conditions, with the only major difference being grain size. The LPO of calcite in torsion and simple shear appear to differ, which may be partly responsible for recrystallization occurring at lower strains in simple shear than in torsion. Grain aspect ratios (a/c) are larger than predicted by theory and the angle between the shear direction and the major axis of the strain ellipse is smaller, consistent with grains behaving as high viscosity particles within a low viscosity matrix. The strength calculated from the flow law for synthetic marble with 30 wt% quartz in torsion matched the strengths observed in this study the best, as expected. The strength was underestimated by the Solnhofen limestone flow law, even more so by the Carrara marble flow law, and the Yule marble flow law was the worst match, also as expected. Paleostresses calculated from dislocation densities using previously developed paleopiezometers were within 12% of the actual stresses, which is excellent agreement. Finally, recrystallized grain size piezometers suggest that the synthetic marble undergoes rotation recrystallization, rather than migration recrystallization, which is consistent with findings from the aspect ratio and SPO observations that grains rotate relative to the boundaries. The paleowattmeter and paleopiezometer were difficult to apply due to small sample size, and it is still

unknown which is more applicable to this material. Overall, there is some evidence that the loading conditions play a significant role in the observed material strength because of the effects on slip systems and LPO. The results of this initial survey suggest that future work towards relating loading geometry and material strength is recommended. Systematic studies of the deformation mechanisms, LPO, active slip systems, and flow law parameters for the same material in torsion, simple shear, and triaxial loading would be ideally suited to resolving this issue.

REFERENCES

AUSTIN, N., & EVANS, B. 2007. Paleowattmeters: A scaling relation for dynamically recrystallized grain size. *Geology*, 56, 343-346.

AUSTIN, N., EVANS, B., HERWEGH, M., & EBERT, A. 2008. Strain localization in the Morcles Nappe. *Swiss Journal of Geosciences*, 101, 341-360.

BARNHOORN, A., BYSTRICKY, M., BURLINI, L., KUNZE, K. 2004. The role of recrystallisation on the deformation behaviour of calcite rocks: large strain torsion experiments on Carrara marble. *Journal of Structural Geology,* 26, 885-903.

BEHRMANN, J. H. 1983. Microstructure and fabric transitions in calcite tectonites from the Sierra Alhamilla (Spain). *Geologische Rundschau,* 72, 605-618.

BESTMANN, M., KUNZE, K. & MATTHEWS, A. 2000. Evolution of a calcite marble shear zone complex on Thassos Island, Greece: microstructural and textural fabrics and their kinematic significance. *Journal of Structural Geology,* 22, 1789-1807.

BILBY, B.A., GARDNER, L.T.A. , & SMITH, E. 1958. "The Relation Between Dislocation Density and Stress." *Acta Met.*

BIRD, J.E., MUKHERJEE, & A.K., DORN, J.E. 1969. Correlations Between High-Temperature Creep Behavior and Structure.

BRIEGEL, U. & GOETZE, C. 1978. Estimates of differential stress recorded in the dislocation structure of Lochseiten Limestone (Switzerland). *Tectonophysics,* 48, 61-76.

BRODIE, K. H. & RUTTER, E. H. 2000. Deformation mechanisms and rheology; why marble is weaker than quartzite. *Journal of the Geological Society, London,* 157, 1093-1096.

BROMLEY, R. & SELLARS, C.M. 1973. "High Temperature Deformation of Cu and Cu-Al Alloys." Proc. Conf. on Microstructure and Design of Alloys, Institute of Metals and Iron and Steel Institute, London. 1, (78), 380-385 (1973)

BURKHARD, M. 1990. Ductile deformation mechanisms in micritic limestones naturally deformed at low temperatures (150-350°C). *In:* KNIPE, R. J. &
BUSCH, J. P. & VAN DER PLUIJM, B. A. 1995. Calcite textures, microstructures and rheological properties of marble mylonites in the Bancroft shear zone, Ontario, Canada. *Journal of Structural Geology,* 17, 677-688.

BUSCH, J. P. & VAN DER PLUIJM, B. A. 1995. Calcite textures, microstructures and rheological properties of marble mylonites in the Bancroft shear zone, Ontario, Canada.

Journal of Structural Geology, 17, 677-688.

CASEY, M., KUNZE, K., OLGAARD, D.L. 1998. Texture of Solnhofen limestone deformed to high strains in torsion. *Journal of Structural Geology,* 20, 255-267.

COVEY-CRUMP, S. J. & RUTTER, E. H. 1989. Thermally-induced grain growth of calcite marbles on Naxos Islands, Greece. *Contributions to Mineralogy and Petrology,* 101, 69-86.

DE BRESSER, J. H. P. & SPIERS, C. J. 1990. High-temperature deformation of calcite single crystals by r + and f+ slip). *In:* KNIPE, R. J. & RUTTER, E. H. (eds) *Deformation mechanisms, rheology and tectonics.* Geological Society, London, Special Publications, 54, 285-298.

DE BRESSER, J. H. P. 1991. Intracrystalline deformation of calcite. *Geologica Ultraiectina,* 79 (PhD thesis, Utrecht University, the Netherlands).

DE BRESSER, J. H. P. & SPIERS, C. J. 1993. Slip systems in calcite single crystals deformed at 300-800 °C. *Journal of Geophysical Research,* 98, 6397-6409.

DE BRESSER, J. H. P. 1996. Steady state dislocation densities in experimentally deformed calcite materials; single crystals versus polycrystals. *Journal of Geophysical Research,* 101(10), 22189- 22201.

DE BRESSER, J.H.P., PEACH, C.J., REIJS, J.P.J. & SPIERS, C.J. 1998. On dynamic recrystallization during solid state flow: Effects of stress and temperature, *Geophys. Res. Lett.*, 25, 3457–3460.

DE BRESSER, J., TER HEEGE, J., & SPIERS, C. 2001. Grain size reduction by dynamic recrystallization: can it result in major rheological weakening? *International Journal of Earth Sciences* 91, 28-45.

DE BRESSER, J., EVANS, B., & RENNER, J. 2002. On estimating the strength of calcite rocks under natural conditions. *Geological Society, London, Special Publications*, 22, 309-329.

DRURY, M. R. & URAI, J. T. 1990. Deformation-related recrystallization processes. *Tectonophysics,* 172, 235-253.

GLOVER, G., & SELARS, C.M. 1973. Recovery and recrystallization during high temperature deformation of α-iron. *Metallurgical and Materials Transactions B*, 4, 765-775.

GOETZE, C., & KHOLSTEDT, D.L. 1977. The dislocation structure of experimentally deformed marble. *Contributions to Mineralogy and Petrology*, 59, 293-306.

HEARD, H. C. & RALEIGH, C. B. 1972. Steady-state flow in marble at 500 to 800 °C. Geological Society of America, Bulletin, 83, 935-956.

HEITZMANN, P. 1987. Calcite mylonites in the central Alpine 'root zone'. *Tectonophysics,* 135, 207-215.

HERWEGH, M., & KUNZE, K. 2002. The influence of nano-scale second-phase particles on deformation of fine grained calcite mylonites. *Journal of Structural Geology*, 24, 1463-1478.

HIRTH, G., TEYSSIER, C., & DUNLAP, J.W. 2001. An evaluation of quartzite flow laws based on comparisons between experimentally and naturally deformed rocks. *International Journal of Earth Sciences*, 90, 77-87.

KENNEDY, L. A. & LOGAN, J. M. 1997. The role of veining and dissolution in the evolution of fine-grained mylonites; the McConnell Thrust, Alberta. *Journal of Structural Geology,* 19, 785-797.

KHOLSTEDT, D.L., & WEATHERS, M. S. 1980. Deformation-Induced Microstructures, Paleopiezometers, and Differential Stresses in Deeply Eroded Fault Zones. *J. Geophys. Res.*, *85*(B11), 6269–6285.

KOHLSTEDT, D. L., EVANS, B. & MACKWELL, S. J. 1995. Strength of the lithosphere: constraints imposed by laboratory experiments. *Journal of Geophysical Research,* 100, 17587-17602.

LUTON, M.J., & SELLARS, C.M. 1969. Dynamic Recrystallization in Nickel and Nickel-Iron Alloys During High-Temperature Deformation. *Acta Metalurgica*, 17, 1033-1043.

MERCIER, J.C., ANDERSON, & D.A., CARTER, N.L. 1977. Stress in the lithosphere: Inferences from steady state flow of rocks. *Pure and Applied Geophysics*, 115, 199-226.

MOLLI, G., CONTI, P., GIORGETTIC, G., MECCHERI, M. & OSTERLING, N. 2000. Microfabric study on the deformational and thermal history of the Alp Apuane marbles (Carrara marbles), Italy. *Journal of Structural Geology,* 22, 1809-1825.

PFIFFNER, O. A. 1982. Deformation mechanisms and flow regimes in limestone from the Helvetic zone of the Swiss Alps. *Journal of Structural Geology,* 4, 429-444.

PFIFFNER, O. A. & RAMSAY, J. G. 1982. Constraints on geological strain rates; arguments from finite strain states of naturally deformed rocks. *Journal of Geophysical Research,* 87, 311-321. transition. *Journal of Structural Geology,* 21, 351-369.

PIERI, M., BURLINI, L., KUNZE, K., STRETTON, I. & OLGAARD, D. L. 2001. Rheological and micro structural evolution of Carrara Marble with high shear strain;

results from high temperature torsion experiments. *Journal of Structural Geology,* 23, 1393-1413.

POIRIER, J.P., & GUILLOPE, M., 1979. Deformation induced recrystallization of minerals. *Bull. Mineral.*, 102, 67-74.

POST, A., & TULLIS, J. 1999. A recrystallized grain size piezometer for experimentally deformed feldspar aggregates. *Tectonophysics,* 303, 159-173.

RENNER, J. & EVANS, B. 2002. Do calcite rocks obey the power-law creep equation? *In:* DE MEER, S., DRURY, M. R., DE BESSER, J. H. P. & PENNOCK, G. M. (eds) *Deformation Mechanisms, Rheology and Tectonics: Current Status and Future Perspectives,* Geological Society, London, Special Publications, 200, 293-307.

RENNER, J., EVANS, B., & SIDDIQI, G. 2002. Dislocation creep of calcite. *Journal of Geophysical Research,* 107, 6-1 – 6-16.

RENNER, J., SIDDIQI, G., & EVANS, B. 2007. Plastic flow of two-phase marbles. *Journal of Geophysical Research,* 112, 7202-7219.

RUTTER, E. H. 1974. The influence of temperature, strain rate and interstitial water in the experimental deformation of calcite rocks. *Tectonophysics,* 22, 3t 1-334.

RUTTER, E. H. 1995. Experimental study of the influence of stress, temperature, and strain on the dynamic recrystallization of Carrara Marble. *Journal of Geophysical Research,* 100, 24651-24663.

RUTTER, E. H. & BRODIE, K. H. 1988. The role of tectonic grain size reduction in the rheological stratification of the lithosphere. *International Journal of Earth Science,* 77, 295-307.

RYBACKI, E., PATERSON, M., WIRTH, R., & DRESEN, D. 2003. Rheology of calcite – quartz aggregates deformed to large strain in torsion. *Journal of Geophysical Research,* 108, 8-1 - 8-16.

SAKAI, T., & JONAS, J. J. 1984. Dynamic recrystallization: Mechanical and microstructural considerations. *Acta Metallurgica*, 32, 189-209.

SCHMID, S.M., BOLAND, J.N., & PATERSON, M.S. 1977. Superplastic flow in finegrained limestone. *Techtonophysics, 43,* 255-291.

SCHMID, S.M.M PATERSON, M.S., & BOLAND, J.N. 1980. High temperature flow and dynamic recrystalliation in Carrara marble. *Techtonophysics, 65,* 245-280.

SCHMID, S. M., PANOZZO, R. & BAUER, S. 1987. Simple shear experiments on calcite rocks; theology and microfabric. *Journal of Structural Geology, 9,* 747-778.

SHIMIZU, I. 1998. Stress and temperature dependence of recrystallized grain size: A subgrain misorientation model. *Geophys. Res. Lett.*, 25, 4237-4240.

STRIPP, M., TULLIS, J., & BEHRENS, H. 2006. Effect of water on the dislocation creep microstructure and flow stress of quartz and implications for the recrystallized grain size piezometer. *Journal of Geophysical Research*, 111

TWISS, R. J. 1977. Theory and applicability of a recrystallised grain size paleopiezometer. *Pure and Applied Geophysics,* 115, 227-244.

ULRICH, S., SCHULMANN, K. & CASEY, M. 2002. Microstructural evolution and rheological behaviour of marbles deformed at different crustal levels. *Journal of Structural Geology, 24,* 979-995.

UNDERWOOD, E. E. 1970. Quatitative stereology. *Addison-Wesley-Longman*, Reading, Mass.

VAN DER PLUIJM, I. A. 1991. Marble mylonites in the Bancroft shear zone, Ontario, Canada; microstructures and deformation mechanisms. *Journal of Structural Geology,* 13, 1125-1135.

WALKER, A. N., RUTTER, E. H. & BRODIE, K. H. 1990. Experimental study of grain-size sensitive flow of synthetic, hot-pressed calcite rocks. *In:* KNIPE, R. J. & RUTTER, E. H. (eds) *Deformation mechanisms, rheology and tectonics.* Geological Society, London, Special Publications, 54, 259-284.

WHITE, S. 1979. Grain and sub-grain size variations across a mylonite zone. *Contributions to Mineralogy and Petrology*, 7, 193-202.